Ring polymer dynamics and tumbling-stretch transitions in planar mixed flows

Charles D. Young, June R. Qian, Michael Marvin, and Charles E. Sing

Phys. Rev. E **99**, 062502 — Published 10 June 2019

DOI: 10.1103/PhysRevE.99.062502

Ring polymer dynamics and tumbling-stretch transitions in planar mixed flows

Charles D. Young,[1, a)] June R. Qian,[1] Michael Marvin,[2] and Charles E. Sing[1, b)]
[1)] *Department of Chemical and Biomolecular Engineering, University of Illinois at Urbana-Champaign, Urbana, Illinois 61801, USA*
[2)] *Hyland Software, Westlake, OH 44145, USA*

(Dated: 23 May 2019)

The properties of dilute polymer solutions are governed by the conformational dynamics of individual polymers which can be perturbed in the presence of an applied flow. Much of our understanding of dilute solutions comes from studying how flows manipulate the molecular features of polymer chains out-of-equilibrium, primarily focusing on linear polymer chains. Recently there has been an emerging interest in the dynamics of non-linear architectures, particularly ring polymers, which exhibit surprising out-of-equilibrium dynamics in dilute solutions. In particular, it has been observed that hydrodynamics can couple to topology in planar elongational and shear flows, driving molecular expansion in the non-flow direction that is not observed for linear chains. In this paper, we extend our understanding of dilute ring polymer dynamics to *mixed flows*, which represent flow profiles intermediate between simple shear or planar elongation. We map the conformational behaviors at a number of flow geometries and strengths, demonstrating transitions between coiled, tumbling, and stretched regimes. Indeed, these observations are consistent with how linear chains respond to mixed flows. For both linear and ring polymers, we observe a marked first-order-like transition between tumbling and stretched polymers that we attribute to a dynamic energy barrier between the two states. This manifests as bimodal extension distributions in a narrow range of flow strengths and geometries, with the primary difference between rings and linear chains being the presence of molecular expansion in the vorticity direction.

I. INTRODUCTION

The conformational dynamics of individual polymer chains govern the rheological properties of macromolecular fluids, motivating decades of research into developing molecular theories or single-molecule measurements that can elucidate the molecular response to an applied flow.[1] The resulting picture of polymer dynamics, both in and out-of-equilibrium, can now explain a wide variety of polymer dynamical phenomena; for example, sophisticated theories can describe the dynamics of both dilute and concentrated polymers, both in their bulk rheological response[2,3] as well as the implications for molecular conformation.[4] These predictions are consistent with simulation results, as well as single-molecule and bulk experiments.[4] Inspired by these successes, a significant amount of recent research has sought to extend these results for *linear* polymers to *non-linear* polymer architectures such as branched[5] or ring polymers.

Ring polymers are of particular interest to the community, in part due to their ramifications for biomacromolecules such as genomic DNA,[6–8] which is known to exhibit ring-like chain statistics. Rings are also useful model systems for studying the role of polymer chain topology in polymer melts, where the absence of chain 'ends' affects the nature of molecular entanglements between chains.[9,10] The dynamic slowing observed in ring polymer melts is indeed qualitatively different from entangled rings[11–14] and has spurred significant theoretical efforts to understand the connection between molecular conformations and material rheology.[10,15] This has consequently led to experimental studies of the rheological[11,16] properties of ring polymer melts; however, the importance and difficulties in synthesizing 'pure' rings[17] makes this an unresolved question in polymer physics.

Clues to conformational dynamics and material properties in ring polymers can also be found in non-concentrated ring polymer solutions. For example, single molecule experiments have demonstrated that diffusion of a trace ring or linear polymer in semidilute solution depends on the topology of the background solution molecules.[18] In this case, the intermolecular uncrossability of polymer rings is implicated in the chain dynamics, which are prohibited from conformations where two or more rings concatenate. However, it is now appreciated that ring constraints also play a large role in the *intra*-molecular interactions within the ring polymer.[19,20] These will play a significant role in the dilute solution structure and dynamics of ring polymers. For example, rings can contain topological knots, which cannot 'un-tie' and thus exhibit non-trivial conformational structure and dynamics.[21–23]

Recent works by ourselves and others have demonstrated that, even in the absence of these topological features, ring connectivity constraints lead to altered out-of-equilibrium polymer dynamics when compared to linear polymer chains.[23–29] This is apparent in experimental single-molecule studies, which show that there is a delayed coil-stretch transition in planar extensional flow for ring polymers;[19,20] in simulation, this was attributed to cooperative hydrodynamic back-flows between the two stretching 'strands' of the rings that aid in molecular relaxation. More pronounced is the non-flow (for planar

[a)] *These authors contributed equally to this manuscript.
[b)] Electronic mail: cesing@illinois.edu

extension) or vorticity (for shear flow[23]) direction extension of individual rings. This surprising result is due to the geometry of the hydrodynamic back-flows, which drive the two adjacent stretching strands in what we will refer to as the z-direction (with the planar flows occuring in the x-y-plane).

Despite this progress, there remain aspects which have been studied in-depth for linear polymers but not rings. One significant case is in planar mixed flows, which represent flow profiles that are a linear combination of simple shear and planar elongation described by a mixing parameter α. These flows generally represent the more complicated types of situations possible in real processing flows, and for linear polymers exhibit non-trivial effects associated with the transition between a variety of conformational dynamics related to the limiting flow profiles. For example, in the limit of a planar elongational flow ($\alpha = 1$), a linear polymer is known to undergo a sharp transition from a coiled to a highly-stretched state.[30,31] This transition is known to be weakly first-order, exhibiting hysteresis at large polymer lengths.[30,32] To contrast, in strong shear flows ($\alpha = 0$) a linear polymer will tumble between slightly-stretched and coiled conformations.[33] When these two flow types are mixed, with $0 < \alpha < 1$, either of these conformational behaviors - tumbling or stretched conformations - can be observed, with a transition between the two at high flow strengths. This variety of coil-stretch transitions has been widely characterized in theory,[30,34] numerical calculations, Brownian dynamics simulations,[35–38] and single-molecule measurements for linear chains.[35] However, there remains no comprehensive picture of how *ring polymers* behave in similar flows, despite individual efforts to understand the limiting flow types.

In this paper, we use Brownian dynamics (BD) simulations to characterize the out-of-equilibrium dynamics of dilute ring polymers in the presence of planar mixed flows. We contrast rings to similarly-sized linear polymers, and demonstrate that the z-direction expansion observed for rings in pure elongation or shear is similarly observed in planar mixed flows. Additionally, we create a non-equilibrium phase map in $\alpha - \mathrm{Wi}$ space where tumbling, extended, and coiled conformations are present that is analogous to the behavior of linear chains. We further note the presence of a first-order-like transition between tumbling and extended conformations, as evidenced by bimodal distributions in the extension length of the chain in both ring and linear polymers. This transition becomes sharp as the strength of the shear portion of the flow increases, which we attribute to the emergence of a dynamic barrier between the two states. In ring polymers, this bimodal distribution is also observed in the vorticity direction, which we show is coupled to the extensional direction. This work shows that the subtle conformational differences between ring and linear polymers are observed in mixed flows, such as the vorticity direction stretching of the chain. This demonstrates that these phenomena are general, and may play an important role as polymer molecules increase and the presence of these 'stretched' conformations may promote threading or hooking in surprising ways, with ramifications on rheological properties.[39]

II. SIMULATION METHOD

We perform steady state Brownian dynamics simulations of individual flexible ring polymers in dilute solution consisting of N coarse-grained beads i at positions $\boldsymbol{r}_i$. Bead trajectories evolve according the the Langevin equation:[1]

$$\frac{d\tilde{\boldsymbol{r}}_i}{d\tilde{t}} = -\sum_j \tilde{\boldsymbol{\mu}}_{ij} \nabla_{\tilde{\boldsymbol{r}}_j}(\tilde{U}) + \tilde{\boldsymbol{\Gamma}} \cdot (\tilde{\boldsymbol{r}}_i - \tilde{\boldsymbol{r}}_{CoM}) + \tilde{\boldsymbol{\xi}}_i \qquad (1)$$

where tildes indicate dimensionless quantities. Distances are normalized by the bead radius ($\tilde{\boldsymbol{r}}_i = \boldsymbol{r}_i/a$), energies by k_BT ($\tilde{U} = U/(k_BT)$, times by the single bead diffuse time ($\tilde{t} = t/\tau_0$, where $\tau_0 = 6\pi\eta a^3/(k_BT)$ and η is the solvent viscosity), and the mobility tensor by the drag coefficient of the spherical beads ($\tilde{\boldsymbol{\mu}}_{ij} = \boldsymbol{\mu}_{ij}/(6\pi\eta a)$). We have omitted terms involving the spatial gradient of the mobility tensor because we use the Rotne-Prager-Yamakawa (RPY) tensor, which has a zero spatial gradient:[40,41]

$$\tilde{\boldsymbol{\mu}}_{ij} = \begin{cases} \boldsymbol{I}, & i = j \\ \dfrac{3}{4r_{ij}}\left[\left(1 + \dfrac{2}{3\tilde{r}_{ij}^2}\right)\boldsymbol{I} + \left(1 - \dfrac{2}{\tilde{r}_{ij}^2}\right)\hat{\boldsymbol{r}}_{ij}\hat{\boldsymbol{r}}_{ij}\right], & i \neq j, \tilde{r}_{ij} \geq 2 \\ \left(1 - \dfrac{9\tilde{r}_{ij}}{32}\right)\boldsymbol{I} + \dfrac{3\tilde{r}_{ij}}{32}\hat{\boldsymbol{r}}_{ij}\hat{\boldsymbol{r}}_{ij}, & i \neq j, \tilde{r}_{ij} \leq 2 \end{cases} \qquad (2)$$

where $\tilde{r}_{ij} = |\tilde{\boldsymbol{r}}_j - \tilde{\boldsymbol{r}}_i|$ and $\hat{\boldsymbol{r}}_{ij} = \tilde{\boldsymbol{r}}_{ij}/\tilde{r}_{ij}$. Beads interact via bonded and excluded volume (EV) interactions, $\tilde{U} = \tilde{U}^{bond} + \tilde{U}^{EV}$. For the bonded potential we use a Hookean spring with a large spring constant $\tilde{\kappa} = 200$ so that the beads are connected by stiff springs:

$$\tilde{U}^{bond} = \sum_{i=2}^{N} \frac{\tilde{\kappa}}{2}(\tilde{r}_{i,i-1} - 2)^2 \qquad (3)$$

For EV we use a Lennard-Jones (LJ) potential:

$$\tilde{U}^{LJ} = \tilde{u} \sum_{i>j} \left[\left(\frac{2}{\tilde{r}_{ij}}\right)^{12} - 2\left(\frac{2}{\tilde{r}_{ij}}\right)^{6}\right] \qquad (4)$$

where the strength of interaction $\tilde{u} = 0.31$ is chosen so that the chain statistics are representative of a θ-solvent.[42] The applied flow is described by the velocity gradient tensor:

$$\tilde{\boldsymbol{\Gamma}} = \tilde{\dot{\gamma}} \begin{bmatrix} 0 & 1 & 0 \\ \alpha & 0 & 0 \\ 0 & 0 & 0 \end{bmatrix} \qquad (5)$$

where $\tilde{\dot{\gamma}}$ is the shear rate and α is the mixed flow parameter. For $\alpha = 0$ there is simple shear and for $\alpha = 1$ there is planar extension with the axis of extension rotated by an angle $\pi/4$ from the x-axis (see Figure 1 for schematic examples). This form is convenient for varying the ratio of vorticity to extension, which is critical for understanding the polymer conformation.[35–37] A linear chain undergoes a transition from coiled elliptic rotation to cyclic tumbling to a stretched conformation over a narrow range around $\alpha = 0$ where vorticity and extension are equal.[35,36]

The random velocity $\tilde{\boldsymbol{\xi}}_i$ is a Gaussian random variable which satisfies the fluctuation-dissipation theorem $\langle \boldsymbol{\xi}_i(t)\boldsymbol{\xi}_j(t')\rangle = 2k_BT\boldsymbol{\mu}_{ij}\delta(t-t')$ and $\langle \xi_i(t)\rangle = 0$.[1] The decomposition $\boldsymbol{\mu}_{ij} = \mathbf{B}\mathbf{B}^T$ is accomplished by Cholesky decomposition. We numerically integrate Equation 1 by an Euler update with a time step $\Delta\tilde{t} = 1\times10^{-4}$, and the mobility tensor and decomposition are updated every 5 time steps.

Our simulations consider ring and linear polymers of length $N = 120$ at a variety of values of the Weissenburg number $\mathrm{Wi} = \dot{\gamma}\tau_Z$, which is a dimensionless flow rate where the shear rate $\dot{\gamma}$ is normalized by the longest Zimm relaxation τ_Z of either the ring or the linear chain. We use different values of τ_Z for linear and ring polymers, which we determine via the autocorrelation of the molecular extension $\langle \Delta x(t)\cdot\Delta x(t+T)\rangle = Ae^{(-T/\tau_Z)}+B$. Here, $\Delta x = \max(\{x_i\})-\min(\{x_i\})$ is the maximum span of the molecule in the x direction, and the autocorrelation function is determined from equilibrium simulations that are run for 100 relaxation times. We note that at equilibrium the polymer conformation is isotropic and the maximum span in any direction would yield the same result. We demonstrated in previous work that this reproduces the expected relaxation time scaling for both rings and linear chains of varying N,[20] and our value of $\tau_{z,linear}(N = 120) = 260\tau_0$ and $\tau_{z,ring}(N = 120) = 100\tau_0$ is consistent with these results. This yields the same relaxation time as the more commonly used end-to-end vector autocorrelation function, which can be obtained from Rouse and Zimm theory.[1] Because the ring polymer lacks chain ends, however, the extension is more clearly defined and easily compared to the linear case. For each shear rate we vary the mixed flow parameter α from 0 to 1 to simulate the change in ring conformational dynamics moving from shear to extensional flow.

III. RESULTS AND DISCUSSION

A. Chain extension

We compare the fractional chain extension for both ring and linear polymers in the extensional and vorticity (or z-) directions, $\langle \Delta x_f/L\rangle$ and $\langle \Delta z_f/L\rangle$ respectively, with a third direction y_f that is perpendicular to both x_f and z_f that has a corresponding fractional chain extension $\langle \Delta y_f/L\rangle$. This latter direction is the compressional direction at $\alpha = 1$ and the flow gradient direction at $\alpha = 0$. The extension in all directions is normalized by the contour length $L/a = 2N$ for the linear polymer, or by half the contour length $L/a = N$ for the ring polymer. The subscripts f on the variables denote that the fractional extension is measured in relation to the principal axis of extension, rather than the Cartesian coordinates x, y, and z. We note that the axis of extension changes with the mixed flow parameter α (Fig. 1), and is found from the positive eigenvalue of the velocity gradient tensor to be at an angle $\tan^{-1}\sqrt{\alpha}$[36] and with basis vectors $\hat{x}_f = (1+\alpha)^{-1/2}\hat{x} + \sqrt{\alpha}(1+\alpha)^{-1/2}\hat{y}$ and $\hat{y}_f = -\sqrt{\alpha}(1+\alpha)^{-1/2}\hat{x}+(1+\alpha)^{-1/2}\hat{y}$, where hats denote unit vectors. We thus project the polymer coordinates onto this appropriate axis before calculating fractional extension.

We plot the fractional extension $\langle \Delta x_f/L\rangle$ for values of $0 \le \alpha \le 1$, for linear chains. This is plotted in Figure 2a. Consistent with prior literature, we observe chain stretching at $\mathrm{Wi} = 1/2$.[30] The pure extensional flow ($\alpha = 1$) exhibits a sharp transition to the fully stretched state, where the fully extended chain reaches a fractional extension of $\langle \Delta x_f/L\rangle \approx 1$. We note that, by using stiff Hookean springs, the chain can stretch beyond this value; we do not expect this to significantly change the location or nature of this coil-stretch transition compared to other choices for springs that are finitely extensible. At the other limit of $\alpha = 0$, there is a much more gradual transition to a more extended state, with an average stretch $\langle \Delta x_f/L\rangle < 1$ even at high values of Wi due to the presence of molecular tumbling. This is in agreement with prior studies of polymer extension in Brownian dynamics simulations and single-molecule measurements.[33] As the value of α is increased, a sharp transition emerges at high Wi to a nearly extended state. This tumbling-stretch transition proceeds to lower values of Wi as α is increased and the elongational component of the mixed flow is increased, in agreement with prior literature on this system.[34–38] Previous arguments attribute this transition to a stabilization of the stretched state, against the possibility that chain alignment drives the chain orientation can fluctuate across an axis where the flow becomes radially inward and thus driving collapse. We also plot in Figure 2b and c the fractional extension in the $\langle \Delta y_f/L\rangle$ and $\langle \Delta z_f/L\rangle$ directions, and demonstrate that the chain similarly contracts in both directions. This is more pronounced in the y_f direction, due to the compressive nature of the flow, but a similar contraction is also observed in the z_f direction at high stretching.

For rings, we plot the fractional extension $\langle \Delta x_f/L\rangle$ in Fig. 3a for the same range of values of α. We observe conformational dynamics that are similar to linear chains for all values of α. As expected from previous work on dilute ring dynamics, pure extensional flows lead to a sharp transition from the coiled to the stretched state while the simple shear flow case shows a gradual increase in extension and a plateau at high Wi associated with tumbling.[20,23] As also observed in linear chains, a tumble-

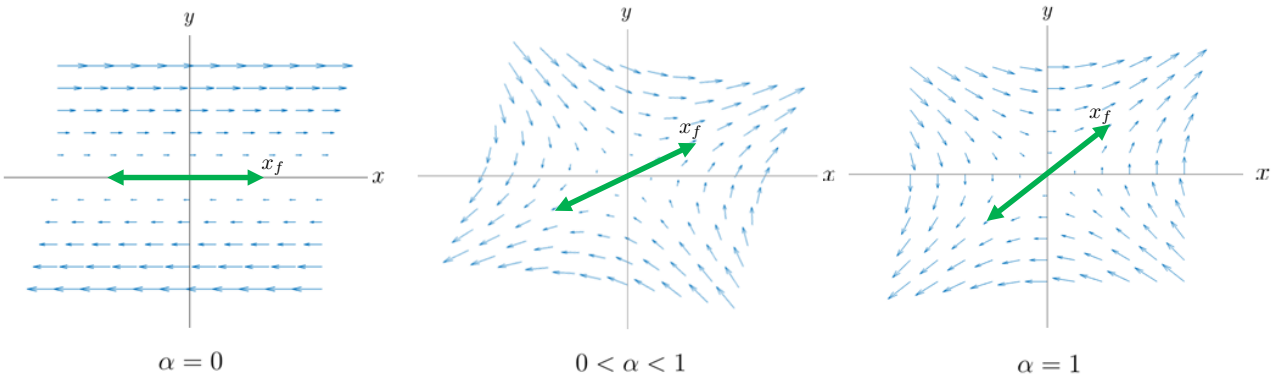

FIG. 1. Mixed flows represent linear combinations of shear flow (leftmost flow field, $\alpha = 0$) and planar elongational flow (rightmost flow field, $\alpha = 1$). Streamlines for various α demonstrate that the principal axis of extension (green arrows denoting x_f) varies in mixed flows $0 < \alpha < 1$.

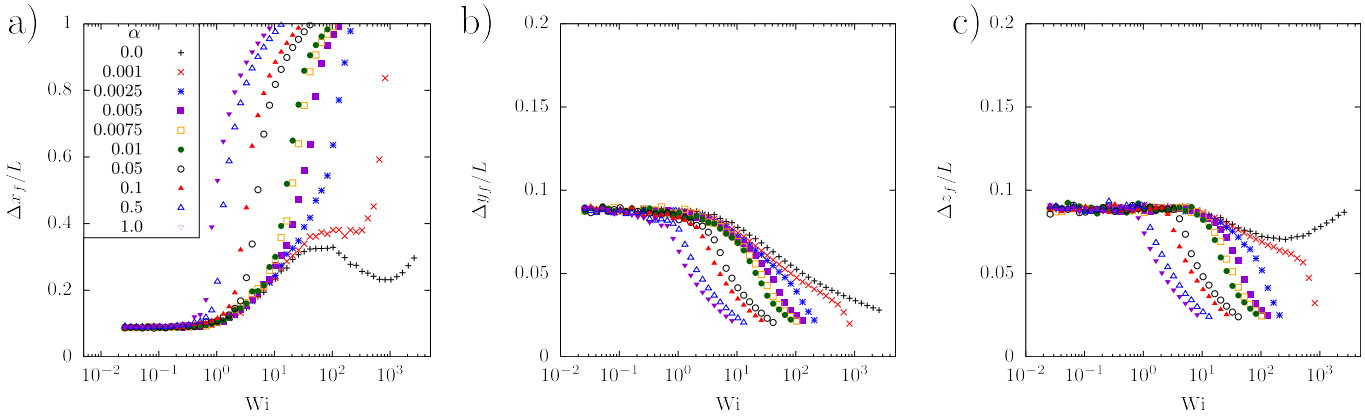

FIG. 2. Linear polymer fractional extension as a function of Weissenburg number and mixed flow parameter α (a) along the axis of principal extension x_f (b) along y_f (c) in the vorticity direction z_f. For the x_f direction, a linear change undergoes a combination of tumbling or stretching depending on Wi and α. Conversely, the chain contracts in both the y_f and z_f directions.

stretch transition emerges at high Wi as α increases away from pure shear flow $\alpha = 0$. As α increases, the critical strain rate required to observe the stretched conformation rather than cyclic tumbling decreases until the transition resembles that of pure extension. We also note the suppression of the dip in $\langle \Delta x_f/L \rangle$ at high Wi in Figure 3a compared to the non-negligible non-monotonicity in Figure 2a. In linear chains, this is a known feature that arises in bead-rod type models, and is attributed to the choice of coarse-grained polymer representation.[43–47] The difference in this feature in ring versus linear chains that we observe is consistent with prior observations that its presence is sensitive to both hydrodynamic and excluded volume interactions.

The largest disparity between ring and linear chains occurs in the values of $\langle \Delta z_f/L \rangle$, which decreases with Wi for linear chains but increases with Wi for rings. This has been observed in both planar extension and shear flow, and is shown to be the result of hydrodynamic backflows.[20,23,29] Theoretical arguments demonstrate that this is primarily due to the z_f-component of these backflows,[20] which is not counteracted by the overall flow and thus acts to stretch the chain in the z_f direction during extension. This does not occur in the y_f-direction, which exhibits the same contracting behavior seen in linear polymer chains for both the y_f and z_f-direction (Figure 2b and c). We indeed observe the z_f stretching behavior in Figure 3b and c, which shows that we observe z_f-direction stretching at *all* values of α at sufficiently strong values of Wi. This effect is more pronounced for strongly extensional flows, so when extension occurs at the tumble-stretch transition there is a concomitant, strong increase in the value of $\langle \Delta z_f/L \rangle$.

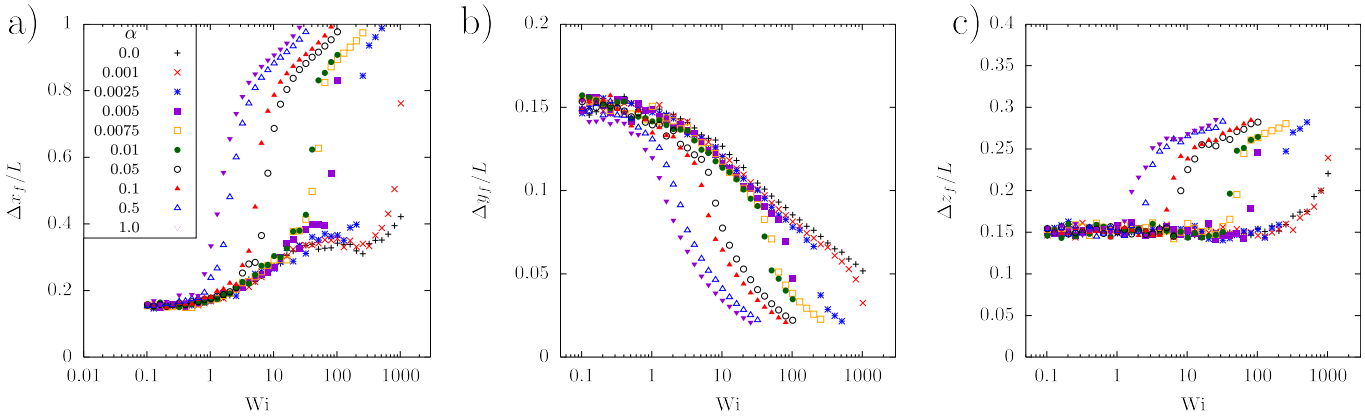

FIG. 3. Ring polymer fractional extension as a function of Weissenburg number and mixed flow parameter α (a) along the axis of principal extension x_f (b) along y_f (c) in the vorticity direction z_f. Similar to the linear case, ring polymers stretch and/or tumble at large Wi in the x_f direction. In contrast to linear chains, however, stretching is observed also in the z_f direction.

B. Conformational phase diagram

We can use the extension data to construct a phase-like diagram mapping the conformational properties of a polymers as a function of the dimensionless flow rate Wi and the mixing parameter α. This is done for both linear and ring polymers in Figure 4a and b respectively. The different regions correspond to the coiled, tumbling, and stretched states, demarcated by transitions and determined via the extension plots in Figure 2 and Figure 3. To define the various regimes, we consider a 'stretched' conformation to have a value of $\langle \Delta x_f/L \rangle > 0.5$, a 'tumbling' conformation with a value of $0.5 > \langle \Delta x_f/L \rangle > 0.2$, and every chain with $\langle \Delta x_f/L \rangle < 0.2$ is considered to be in the coiled conformation. These criteria are not rigorously derived, but instead reflect direct simulation observation.

We note a few features common to the two plots between ring and linear chains. First, at low shear rates (Wi < 0.5), the polymer remains coiled for all values of α. In the limit $\alpha \to 0$ polymers show tumbling behavior at Wi $\approx 2-5$. As $\alpha \to 1$, the polymers undergo a coil-stretch transition around Wi ≈ 0.5. We do note that there is a slight quantitative shift in the coil-stretch Wi at $\alpha = 1$ observed for the ring polymer in Figure 4b compared to Figure 4a, which is consistent with previous reports that the onset of the coil-stretch transition occurs for slightly higher Wi for ring polymers when compared to linear polymers.[19,20] To demonstrate the extent of this shift between the $\alpha = 1$ stretching in the ring and linear case, we plot both the linear and ring polymer fractional extension $\langle \Delta x_f/L \rangle$ as a function of a flow rate Wi in Figure 5; however, the Wi for the linear polymer extension is shifted by a factor β to overlap the ring polymer extension plot. We use the factor $\beta = 1.45$ previously found from experiment[19] and simulation[20] and find good agreement.

While the coil-tumbling and coil-stretch transitions vary only slightly with α, there is a strong dependence for $0 < \alpha < 10^{-2}$. This transition occurs at progressively lower values of Wi for larger α as described previously, and eventually meets with the tumbling transition line to become the coil-stretch transition curve. At low values of α, this transition spans a number of values of Wi, which will be discussed in the next section. We denote this transition region with orange points in Figures 4a and b.

In most of the aforementioned features of these phase diagrams, ring and linear polymers are qualitatively consistent with each other, with only small quantitative differences; we explore these differences more in-depth later in the manuscript. We note that the phase diagrams do not capture the previously-described hydrodynamic stretching in the z-direction.

C. Tumble-stretch transitions in ring and linear polymers

In Figure 4, we represent a number of points as orange symbols around the tumble-stretch transitions, for both ring and linear polymers. These points denote the presence of strong first-order-like transition that is observed in the tumble-stretch behavior of these polymers. Our use of the term 'first-order-like' is inspired by prior work that has used phase transition concepts to understand coexisting conformational states in out-of-equilibrium polymer systems.[30,32,34] These transitions manifest as a rapid but infrequent interconversion between tumbling and stretched states observed in the polymer stretching dynamics, which is demonstrated in Figure 6. Here, the values $\Delta x_f/L$ and $\Delta z_f/L$ are plotted as a function of time for a ring polymer at a series of Wi and $\alpha = 0.001$. These time evolution plots demonstrate the presence of two coexisting dynamic states, one state where the polymer is tumbling with a value of $\Delta x_f/L$ that oscillates within a range of ca. $0.2 < \Delta x_f/L < 0.6$, and one state where the polymer is nearly fully extended at $\Delta x_f/L \approx 0.8 - 1.0$. As the value of Wi is increased

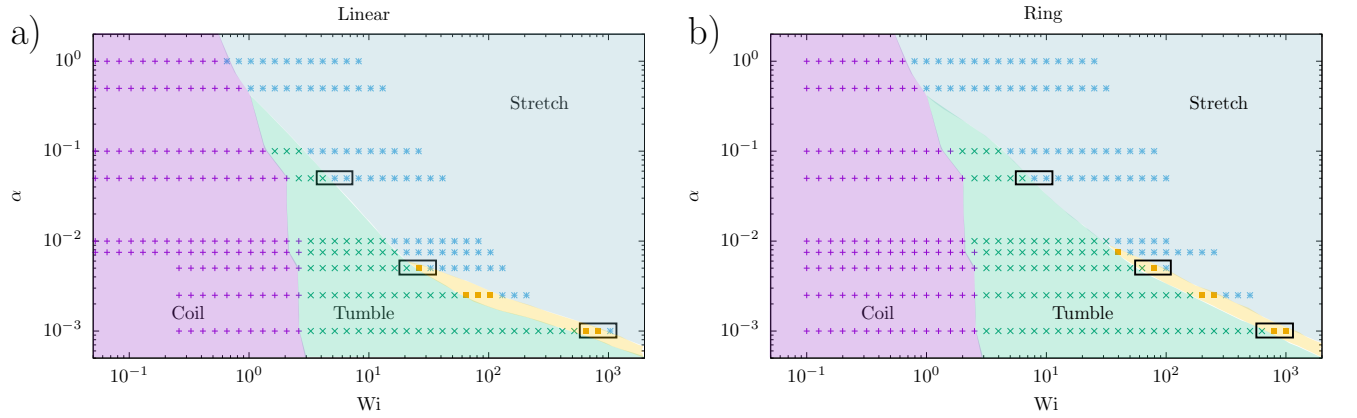

FIG. 4. (a) Linear and (b) ring polymer conformational phase diagrams as a function of strain rate Wi and the mixed flow parameter α. Points correspond to simulations, which are categorized by the criteria described in the text. Coiled chains are near-equilibrium conformations, tumbling chains are rapidly oscillating between slightly-stretched and un-stretched conformations, and fully stretched chains are stable near $\Delta x \approx 0.8 - 1.0$. We find a coexistence-like region, which is colored in orange, where there is a bimodal distribution of chain extensions $\Delta x_f/L$. Boxed points correspond to the probability distribution functions in Figures 7 and 8.

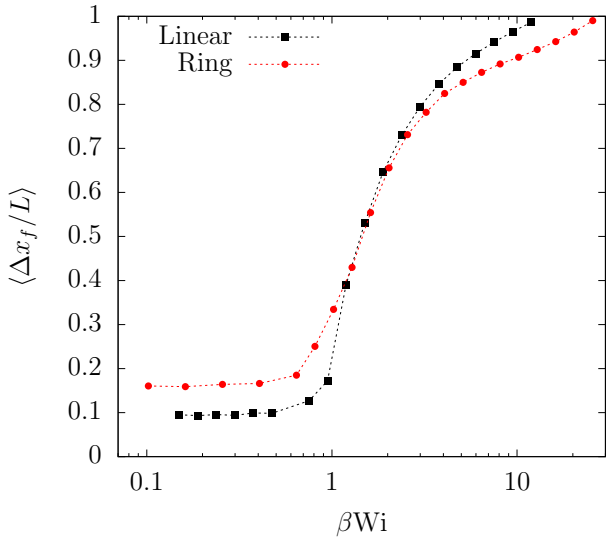

FIG. 5. Fractional extension as a function of shifted βWi for ring and linear polymers with $\alpha = 1$. The linear data is shifted by a factor $\beta = 1.45$, whereas for the ring data $\beta = 1.0$

from Figure 6a-c, the length of time that the polymer spends in the fully extended state increases drastically, with only a few stretching events in Figure 6a that are short-lived, all the way to long-lived extended states in Figure 6c; in these examples, the transition from tumbling to stretching occurs as a transition 'event' much longer-lived than the relaxation time of the molecule. For example, the ring relaxation time $\tilde{\tau}_{z,ring} = 100$ is significantly less than the extended runs of ca. $\tilde{\tau}_{ext} \approx 1000$.

To characterize the nature of this interconversion, we plot three measures of polymer conformation as a function of Wi and α for both linear and ring polymers: (i) the probability distribution functions (PDFs) of the single-chain extension, $P(\Delta x_f/L)$ (Figure 7 and 8) (ii) the probability distribution of extended state lifetimes (Figures 9) (iii) the power spectral density (PSD) of the polymer orientation angle (Figure 10).

We first show the nature of this tumble-stretch transition in the context of probability distribution functions, focusing specifically on values of α and Wi near the tumble-stretch transition denoted by boxes Figures 4a and b. Both linear (Figs. 7a) and ring (8a) PDFs at low values of α show how this transition, with increasing Wi, is characterized by a bimodal distribution of molecular extensions. One of the peaks in the PDF is broad and at relatively low extensions ($0.2 < \Delta x_f/L < 0.6$), which corresponds to the tumbling behavior; the other PDF peak is narrow and around $\Delta x_f/L \approx 1$, which corresponds to the stretched state of the chain. In these low-α plots, this bimodal behavior extends throughout the transition from tumbling to extension, shifting from the tumbling peak being more prominent at lower Wi to the extension peak being more prominent at higher Wi.

At larger values of α, these bimodal PDFs $P(\Delta x_f/L)$ only occur in the center of the transition between the two states, rapidly becoming less pronounced (Figs. 7b and 8b) as α is increased to the point that we do not observe bimodal PDFs anywhere in the tumbling-stretch transition (Figs. 7c and 8c). We thus observe two different types of tumbling-stretch transitions; a first-order-like transition with a coexistence between tumbling and stretch states at low α, and a second-order-like transition where the chain extends rapidly but without any coexistence at higher α. To indicate the location of these different transitions on the phase diagram, we denote conditions where $P(\Delta x_f/L)$ exhibits a bimodal distribution as orange symbols. This thus shows a narrow coexistence region between the tumbling and stretched states, which

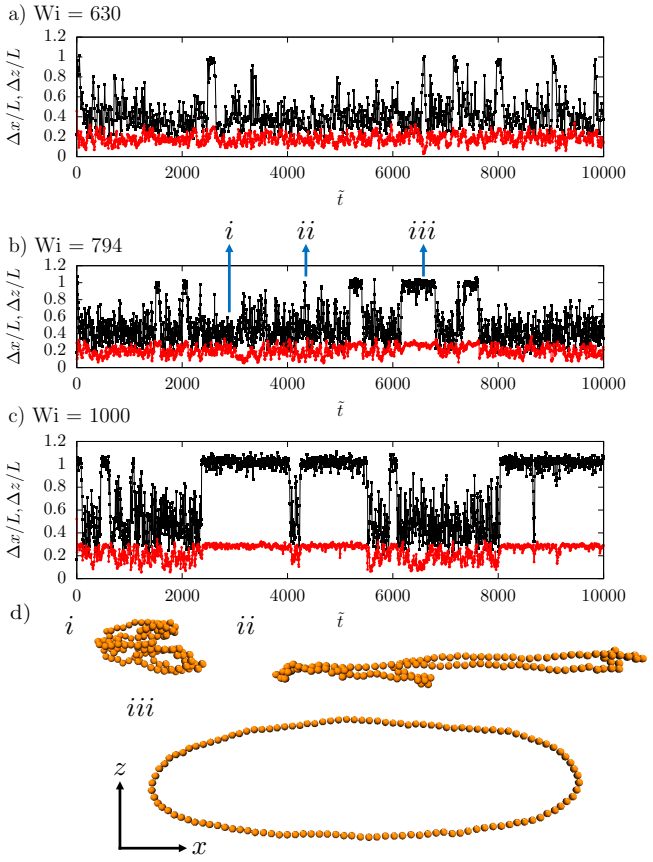

FIG. 6. Simulation traces of ring polymer extension in x_f (black squares) and z_f (red circles) for $\alpha = 0.001$ and (a) Wi = 630 (b) Wi = 794 (c) Wi = 1000 (corresponding to the probability distribution function in 8a). We note the coexistence of two distinct conformational behaviors; a rapidly fluctuating extension length $\Delta x_f/L$ and $\Delta z_f/L$ that corresponds to molecular tumbling, and a stretched conformation at high values of $\Delta x_f/L$ and $\Delta z_f/L$. (d) Snapshots at Wi = 794 are indicated by the numerals in (b), and show the unextended (i) and extended (ii) tumbling rings, and a fully stretched ring (iii).

disappears at a critical value of α.

We further quantify the distinction between stretched and tumbling regions of the phase diagram by characterizing the duration of long-lived extended states that can coexist with tumbling dynamics at the same α-Wi conditions. While the polymer can reach large extensions during the tumbling cycle,[33] these conformations are unstable and will return to the coiled state in the presence of sufficiently strong rotational flow (low α) following a thermal fluctuation away from the axis of principal extension. Typically, they do not survive longer than the characteristic polymer tumbling time scale τ_{tumble}, defined below. In contrast, polymers in the stretched conformation must overcome a relatively large dynamic barrier to collapse and thus survive for time scales much greater than τ_{tumble}. Considering traces of $\Delta x_f/L$ as seen in Figure 6, we define a polymer to be extended when $\Delta x_f/L > \langle \Delta x_f/L \rangle_{min} + 0.1$, where $\langle \Delta x_f/L \rangle_{min}$ is the minimum in the extension PDF, which is generally in the range of 0.6-0.9. Then, we measure the time which a polymer remains extended, τ_{ext}, before returning to a coiled state. We determine the probability distribution of extended state lifetimes, $P(\tau_{ext})$, for slices of the conformational phase diagram passing through the tumble-stretch region.

The distributions $P(\tau_{ext})$ of all $\alpha-$Wi conditions in the tumbling and tumble-stretch region show similar behavior: the highest probability occurs at times shorter than the polymer relaxation time, followed by an exponential decay which is slower for higher α. For $\alpha \geq 0.01$ the polymer remains extended for the duration of the simulation, and thus the distribution is not shown. Examples of these distributions for varying Wi at constant α and varying α at constant Wi for linear polymers are shown in the insets of Figure 9. Ring polymers show qualitatively similar distributions.

Because the distributions $P(\tau_{ext})$ are qualitatively similar, we instead focus on the rate of decay of probability density, λ_{ext}, which is obtained by an exponential fit to the distribution data of the form $P(\tau_{ext}) = Ae^{-\tau_{ext}/\lambda_{ext}}$, where A is a constant. This represents a characteristic lifetime of an extended state, with the limit in the stretched region at high α given by $\lim_{\alpha \to 1} \lambda_{ext} = \infty$.

We find that the characteristic lifetime λ_{ext} is approximately constant at low α and Wi, followed by a sharp increase and divergence at high $\alpha-$Wi approaching the stretched limit. The low $\alpha-$Wi values correspond to rapid tumbling cycles in the tumbling region of the phase diagram, which vary only slightly in frequency. As α and Wi increase, the characteristic lifetime increases as the extended state becomes more stable to fluctuations. For conditions where the characteristic lifetime is very long ($\lambda_{ext} > 10^3 \tau_0$) or not measurable, we consider the polymer to be in the stretched region.

In between these two limiting cases, stretched and tumbling conformations coexist. There are long lasting extended states which cannot be included in the tumbling cycle, but it is also possible to return to the tumbling state by a thermal fluctuation which perturbs the polymer from the principal axis of extension. Notably, these measures are quantitatively consistent with the phase boundaries as determined by the extension PDFs.

In addition to the PDFs and lifetime distribution analysis, we can also quantify the polymer tumbling time scale by a peak in the power spectral density of the polymer orientation angle, which has previously been used to identify characteristic periodic time scales in experiment and simulation.[33] The polymer orientation angle θ is defined as

$$\tan(2\theta) = \frac{2G^f_{xy}}{G^f_{xx} - G^f_{yy}} \tag{6}$$

where G^f_{ij} is the radius of gyration tensor rotated by an angle $\tan^{-1}\sqrt{\alpha}$ consistent with the rotation applied

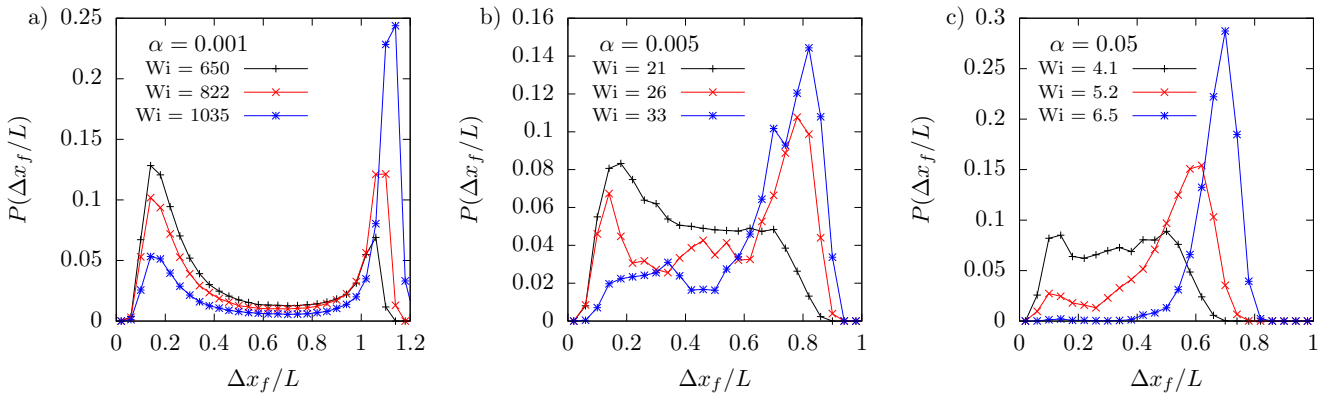

FIG. 7. Probability density function of linear polymer stretch along the principal axis of extension for (a) $\alpha = 0.001$ (b) $\alpha = 0.005$ (c) $\alpha = 0.05$ and selected flow rates Wi. These points are indicated in Figure 4a by boxes.

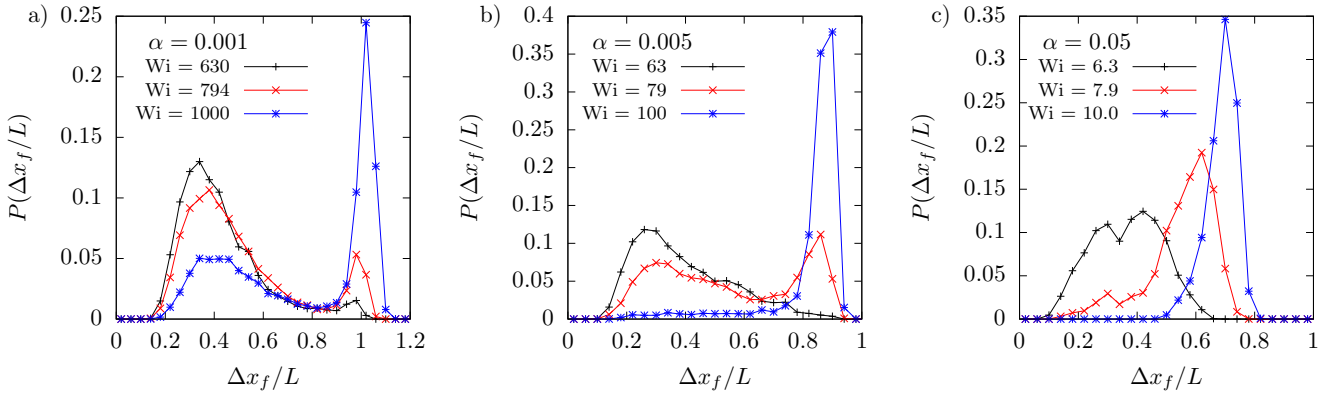

FIG. 8. Probability density function of ring polymer stretch along the principal axis of extension for (a) $\alpha = 0.001$ (b) $\alpha = 0.005$ (c) $\alpha = 0.05$ and selected flow rates. These points are indicated in Figure 4b by boxes.

to the fractional extension data. The gyration tensor is defined as $G_{ij} = \sum_{m=1}^{N} R_i^m R_j^m/N$, where $R_i^m = r_i^m - r_{i,CoM}$ is the displacement in the i direction from the chain center of mass to the position of bead m. The power spectral density (PSD) of the orientation angle $\mathcal{P}(\omega) = \int_{-\infty}^{\infty} C_{\theta,\theta}(T) e^{-2\pi i\omega T} dT$ is the Fourier transform of the time autocorrelation function $C_{\theta,\theta}(T) = \langle\theta(t)\theta(t+T)\rangle$. A peak in the PSD gives the time scale of tumbling. We present the PSD for the same slices in and as in the lifetime distribution analysis. For low α and Wi, there is a clearly identifiable peak. The peak is more pronounced for the ring polymer, as expected because the lack of chain ends restricts the conformational degrees of freedom of the polymer and reduces the diversity of conformations observed during a tumbling cycle. Both cases are qualitatively similar, however. As Wi increases at constant α, the tumbling frequency shifts to the right corresponding to faster tumbling cycles because of the increased flow rate. As α increases at constant Wi, the height of the peak decreases and remains at approximately the same frequency. In this case the rotational component of flow remains comparable so the frequency is constant, but tumbling becomes less common because of enhanced extensional flow, leading to a weaker peak. At sufficiently high α or Wi, the peak is not identifiable, and the PSD is flat on frequencies comparable to the polymer relaxation time. In this case, the orientation angle is similarly correlated for a wide range of frequencies, indicating long-lived extended states as quantified by the lifetime distribution analysis.

The PSD is quantitatively consistent with both the lifetime distribution and extension distribution. The conditions with an identifiable peak correspond to tumbling or tumble-stretch regions of the phase diagram where periodic tumbling occurs. As tumbling becomes rare the peak shifts to the right and vanishes, corresponding to a transition into the stretched region. This transition is less drastic than in the lifetime distribution, but the results are qualitatively similar. Additionally, we see that the tumbling timescale is consistent with lifetime of extended states at low $\alpha-$Wi conditions in the tumbling region. From visual inspection of peaks, the linear polymer tumbling time scale at $\alpha = 0.001$ is $\tau_{tumble} \approx 0.01 - 0.05\tau_Z$ for Wi $= 327 - 1035$. For the ring polymer at $\alpha = 0.005$, we find $\tau_{tumble} \approx 0.3 - 0.5\tau_Z$ for Wi $= 51 - 128$.

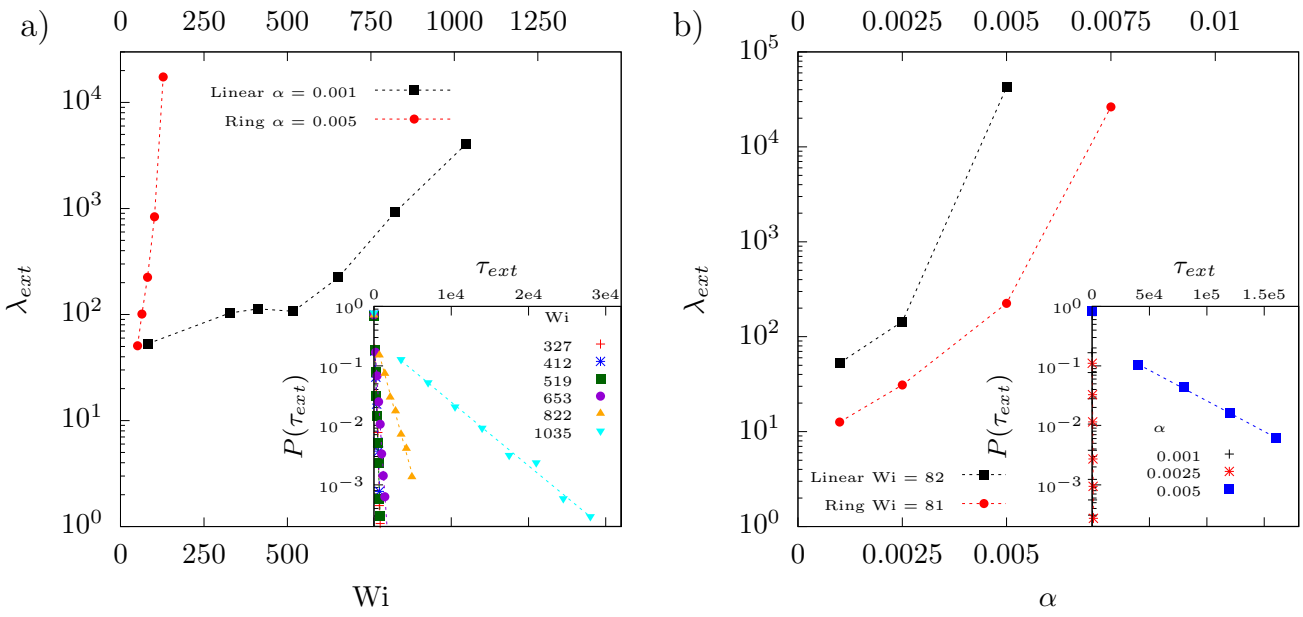

FIG. 9. Characteristic lifetime of an extended state for linear and ring polymers (a) at constant α and varying Wi (b) at constant Wi and varying α. Insets are the probability distribution of extended lifetimes for the linear polymer case and dashed lines are exponential fits via λ_{ext}.

The analogy of the low-α tumble-stretch transition to a first order phase transition suggests the presence of a significant dynamic free energy barrier between the two states. We postulate that this barrier is significant in both the tumble-stretch and stretch-tumble directions, and emerges due to the particular combination of shear and elongational flows present in the mixed system. The stretch-tumble barrier is due to the stabilizing effect of the elongational portion of the mixed flow, which 'stretches' the chain and prevents it from fluctuating into a compression region of the flow field. This argument has been suggested previously, for both linear coils[36] and globules.[38] We attribute the dynamic competition between stretching and tumbling of a coil as the origin of the tumble-stretch barrier, which should increase as the strength of the shear component increases (or as $\alpha \to 0$). In this limit, there is only a limited opportunity for the polymer molecule to accumulate enough strain that it is in a sufficiently 'stretched' conformation before a tumbling event occurs. This opportunity decreases with decreasing α, resulting in an increasing barrier.

In Figures 7 and 8, only quantitative differences are apparent in the distributions $P(\Delta x_f/L)$ for ring versus linear chains. However, we can also consider distributions in the vorticity-direction extension $P(\Delta z_f/L)$ for both linear and ring chains. We plot both types of distributions for both types of chains in Figure 11a, revealing a distinct difference in $P(\Delta z_f/L)$ for linear versus ring chains; namely, the ring chains also exhibit a distribution in $\Delta z_f/L$ that has a shoulder that is commensurate with the bimodal distribution in $\Delta x_f/L$. To contrast, linear chains do not have this same shoulder in the $\Delta z_f/L$ distribution, and instead $P(\Delta z_f/L)$ only shows a single peak at low $\Delta z_f/L$. The shoulder of the distribution in the ring chains is due to the previously described vorticity extension that arises due to hydrodynamic interactions, which occurs when the ring is fully extended in the x-direction. This is apparent in the time-plots of $\Delta z_f/L$ in Figure 6, which exhibit a correlation between the extension in the x_f and z_f directions. This is reinforced by simulation snapshots, with a few examples in Figure 6d shown in the $x-z$ plane and corresponding to indicated points on the time-plots in Figure 6b. Here, snapshots i and ii represent different conformational extremes during the tumbling process, and show very little extension in the z-direction. In Figure 6d, iii, however, the chain stretches considerably in the z-direction.

To quantitatively show the strength of this correlation, we plot in Figure 11b a contour plot of the values of $\Delta x_f/L$ versus $\Delta z_f/L$ sampled over the course of the simulation of both ring and linear chains used to create the probability distribution functions in Figure 11a. In both cases, the probability is non-zero over almost the entire space of Δx_f, but the locations of the high probability regions are distinctly different. For the linear chain in Figure 11b, $P(\Delta x_f/L)$ is only marginally bimodal, so there is a high probability region at high extension $\Delta x_f/L > 0.6$ that is also at low $\Delta z_f/L$. The tumbling state occurs in a more diffuse region of increased probability at low $\Delta x_f/L < 0.6$ and at a slightly higher value of $\Delta z_f/L$. To contrast, the ring polymer in Figure 11b shows two distinct regions of high probability , one at low $\Delta x_f/L$ and low $\Delta z_f/L$, and another at high values of both $\Delta x_f/L$ and $\Delta z_f/L$. This second, high extension

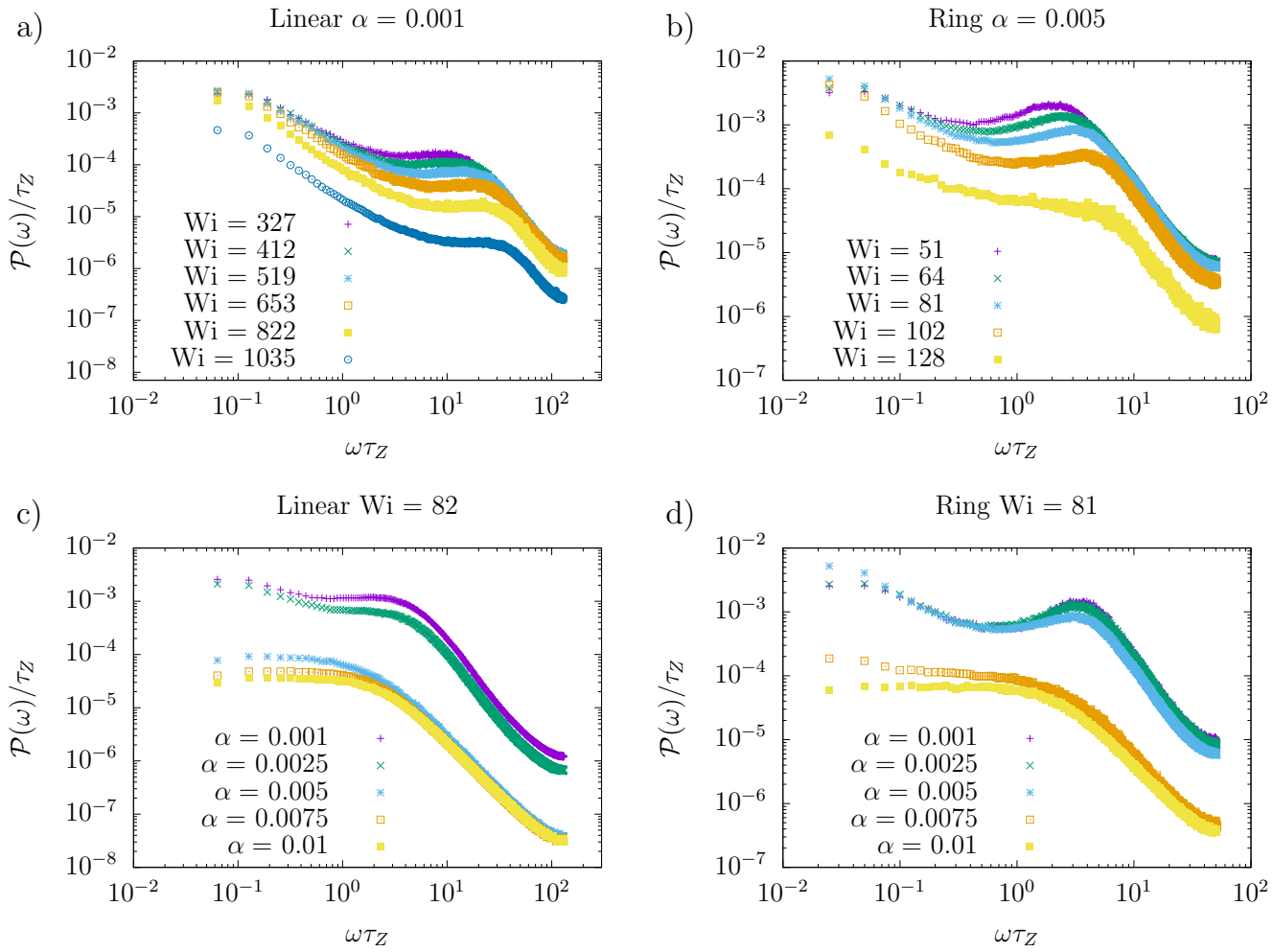

FIG. 10. Power spectral density of the polymer orientation angle for a (a) linear polymer at constant $\alpha = 0.001$ (b) ring polymer at constant $\alpha = 0.005$ (c) linear polymer at constant Wi = 82 (d) ring polymer at constant Wi = 81.

region corresponds to the upper peaks in the bimodal distributions, and shows that extension in both the stretch and vorticity direction are coupled.

IV. CONCLUSIONS

We have mapped out the conformational properties of polymer rings in the presence of mixed planar flows, elucidating a series of intermediate flow states between the limiting cases of simple shear and planar elongation. We demonstrate features similar to those found in linear chains, primarily the presence of a transition between shear-induced tumbling and elongational-induced stretching that occurs at intermediate values of α and Wi. In this regime, we observe the emergence of a bimodal distribution of molecular lengths that we attribute to a first-order-like transition that becomes increasingly pronounced as the value of α is increased. This is observed in both linear and ring polymers. In all ring stretching regimes, we observe the z-direction extension that has previously been reported for limiting shear and elongational flows, and that this is also observed in bimodal conformation distributions that occur at the tumbling-extension transition.

This work shows that topological differences, in particular the coupling of topology to hydrodynamic interactions, can extend beyond the most simple flow profiles and can be observed in increasingly complicated flow situations. This likely affects the behavior of molecular rings in real processing situations, where the nature of polymer-polymer interactions will be governed by their flow-driven conformational properties and subsequently affect rheological properties. Nevertheless, it is unclear how these hydrodynamic effects will extend to non-dilute systems and complicated flows. This work suggests that the extended conformation of ring polymers in a variety of flows may facilitate topological interactions, such as linear-ring or ring-ring threading or hooking in semidilute systems.

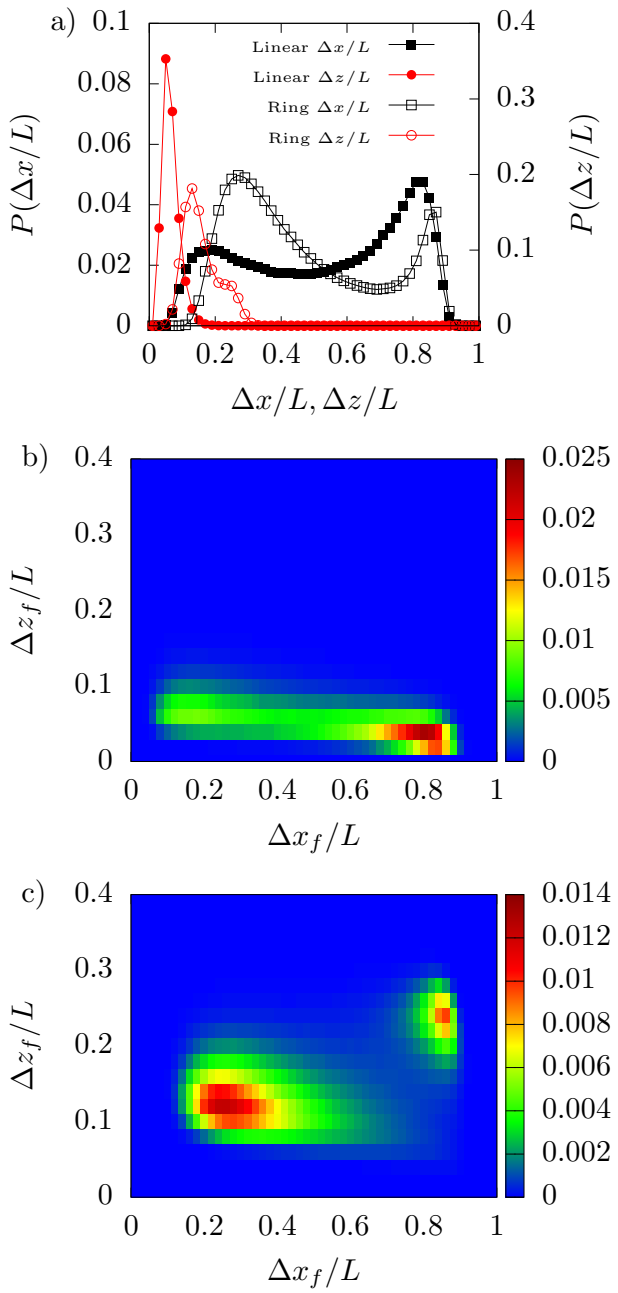

FIG. 11. (a) Probability density function of ring and linear polymer stretch along the principal axis of extension and the vorticity (z_f) direction at $\alpha = 0.005, \mathrm{Wi}_{ring} = 79, \mathrm{Wi}_{linear} = 33$. These points are chosen to have the same α and average extension $\langle \Delta x_f/L \rangle$. Closed points correspond to the linear chain and open to the ring. The $\Delta z_f/L$ distribution has been plotted on a second y-axis. We note a shoulder in the $\Delta z_f/L$ distribution for the ring polymer. (b) Contour plot of $P(\{\Delta x_f/L, \Delta z_f/L\})$ for a linear polymer at $\alpha = 0.005, \mathrm{Wi}_{linear} = 33$ (c) Contour plot of $P(\{\Delta x_f/L, \Delta z_f/L\})$ for a ring polymer at $\alpha = 0.005, \mathrm{Wi}_{ring} = 79$.

ACKNOWLEDGMENTS

This work was supported by the National Science Foundation under award number CBET-1803757. The authors thank Sarit Dutta for intellectual discussions and comments on the manuscript.

[1] M. Doi and S. F. Edwards, *The theory of polymer dynamics* (Oxford University Press, 1988).
[2] R. B. Bird, R. C. Armstrong, O. Hassager, and C. Curtiss, *Dynamics of Polymeric Liquids-Volume 2: Kinetic Theory* (1987).
[3] R. G. Larson, Oxford University Press, New York Oxford **86**, 108 (1999).
[4] C. M. Schroeder, Journal of Rheology **62**, 371 (2018).
[5] D. J. Mai, A. Saadat, B. Khomami, and C. M. Schroeder, Macromolecules **51**, 1507 (2018).
[6] J. A. Semlyen, *Cyclic polymers* (Springer, 2000).
[7] M. Trabi and D. J. Craik, Trends in biochemical sciences **27**, 132 (2002).
[8] T. Sanchez, I. Kulic, and Z. Dogic, Physical review letters **104**, 098103 (2010).
[9] T. McLeish, Science **297**, 2005 (2002).
[10] M. Rubinstein, Physical review letters **57**, 3023 (1986).
[11] M. Kapnistos, M. Lang, D. Vlassopoulos, W. Pyckhout-Hintzen, D. Richter, D. Cho, T. Chang, and M. Rubinstein, Nature materials **7**, 997 (2008).
[12] J. D. Halverson, W. B. Lee, G. S. Grest, A. Y. Grosberg, and K. Kremer, The Journal of chemical physics **134**, 204904 (2011).
[13] J. D. Halverson, W. B. Lee, G. S. Grest, A. Y. Grosberg, and K. Kremer, The Journal of chemical physics **134**, 204905 (2011).
[14] J. D. Halverson, G. S. Grest, A. Y. Grosberg, and K. Kremer, Physical review letters **108**, 038301 (2012).
[15] A. Y. Grosberg, S. K. Nechaev, and E. I. Shakhnovich, Journal de physique **49**, 2095 (1988).
[16] G. McKenna, G. Hadziioannou, P. Lutz, G. Hild, C. Strazielle, C. Straupe, P. Rempp, and A. Kovacs, Macromolecules **20**, 498 (1987).
[17] J. Roovers and P. Toporowski, Macromolecules **16**, 843 (1983).
[18] R. M. Robertson and D. E. Smith, Macromolecules **40**, 3373 (2007).
[19] Y. Li, K.-W. Hsiao, C. A. Brockman, D. Y. Yates, R. M. Robertson-Anderson, J. A. Kornfield, M. J. San Francisco, C. M. Schroeder, and G. B. McKenna, Macromolecules **48**, 5997 (2015).
[20] K.-W. Hsiao, C. M. Schroeder, and C. E. Sing, Macromolecules **49**, 1961 (2016).
[21] A. Narros, A. J. Moreno, and C. N. Likos, Macromolecules **46**, 3654 (2013).
[22] R. Matthews, A. A. Louis, and C. N. Likos, ACS macro letters **1**, 1352 (2012).
[23] M. Liebetreu, M. Ripoll, and C. N. Likos, ACS Macro Letters **7**, 447 (2018).
[24] J. H. Cifre, R. Pamies, M. L. Martínez, and J. G. de la Torre, Polymer **46**, 267 (2005).
[25] W. Chen, J. Chen, and L. An, Soft Matter **9**, 4312 (2013).
[26] W. Chen, J. Chen, L. Liu, X. Xu, and L. An, Macromolecules **46**, 7542 (2013).
[27] W. Chen, Y. Li, H. Zhao, L. Liu, J. Chen, and L. An, Polymer **64**, 93 (2015).
[28] P. S. Lang, B. Obermayer, and E. Frey, Physical Review E **89**, 022606 (2014).
[29] L. Miao, C. D. Young, and C. E. Sing, The Journal of chemical physics **147**, 024904 (2017).
[30] P.-G. de Gennes, The Journal of Chemical Physics **60**, 5030 (1974).
[31] D. E. Smith, H. P. Babcock, and S. Chu, Science **283**, 1724 (1999).
[32] C. M. Schroeder, H. P. Babcock, E. S. Shaqfeh, and S. Chu, Science **301**, 1515 (2003).

[33]C. M. Schroeder, R. E. Teixeira, E. S. Shaqfeh, and S. Chu, Physical review letters **95**, 018301 (2005).
[34]R. Larson and J. Magda, Macromolecules **22**, 3004 (1989).
[35]J. S. Hur, E. S. Shaqfeh, H. P. Babcock, and S. Chu, Physical Review E **66**, 011915 (2002).
[36]N. Woo and E. S. Shaqfeh, The Journal of chemical physics **119**, 2908 (2003).
[37]B. D. Hoffman and E. S. Shaqfeh, Journal of Rheology **51**, 947 (2007).
[38]C. E. Sing and A. Alexander-Katz, The Journal of chemical physics **135**, 014902 (2011).
[39]Y. Zhou and C. M. Schroeder, arXiv preprint arXiv:1805.06303 (2018).
[40]J. Rotne and S. Prager, The Journal of Chemical Physics **50**, 4831 (1969).
[41]H. Yamakawa, The Journal of Chemical Physics **53**, 436 (1970).
[42]A. Alexander-Katz and R. Netz, Macromolecules **41**, 3363 (2008).
[43]C. Sendner and R. Netz, The European Physical Journal E **30**, 75 (2009).
[44]I. S. Dalal, N. Hoda, and R. G. Larson, Journal of Rheology **56**, 305 (2012).
[45]I. Saha Dalal, A. Albaugh, N. Hoda, and R. G. Larson, Macromolecules **45**, 9493 (2012).
[46]M. M. Moghani and B. Khomami, Physical Review Fluids **2**, 023303 (2017).
[47]C. E. Sing and A. Alexander-Katz, Physical review letters **107**, 198302 (2011).